Choice of PP1 catalytic subunit affects neither the requirement for G-actin nor the insensitivity to Sephin1 of PPP1R15A-regulated eIF2αP dephosphorylation

Running title: A tripartite holophosphatase de-phosphorylates eIF2α

Ana Crespillo-Casado[1], Zander Claes[2], Meng S. Choy[3], Wolfgang Peti[3], Mathieu Bollen[2] and David Ron[1*]

[1]Cambridge Institute for Medical Research, University of Cambridge, Cambridge CB2 0XY, United Kingdom

[2]Department of Cellular and Molecular Medicine, KU Leuven, BE-3000 Leuven, Belgium

[3]Department of Chemistry and Biochemistry, University of Arizona, Tucson, Arizona 85721-0041, United States

[*]Corresponding author:
David Ron
Cambridge Institute for Medical Research
University of Cambridge
Cambridge Biomedical Campus
Wellcome Trust/MRC Building
Hills Road
Cambridge CB2 0XY
United Kingdom
Phone 01223 768 940
Email: dr360@medschl.cam.ac.uk

Abstract:

The integrated stress response is regulated by kinases that phosphorylate translation initiation factor 2α and phosphatases that dephosphorylate it. Genetic and biochemical data indicate that the eIF2α-directed holophosphatase - a therapeutic target in diseases of protein misfolding - is comprised of a regulatory, PPP1R15, and a catalytic, Protein Phosphatase 1 (PP1), subunit. However, differing reports have appeared regarding the requirement for an additional co-factor, G-actin, in enabling substrate-specific de-phosphorylation[1-3]. An additional concern relates to the sensitivity of this PP1 holoenzyme to the [(o-chlorobenzylidene)amino]guanidines (Sephin1 or Guanabenz) small molecule proteostasis modulators[3,4]. We find that in the absence of G-actin, PPP1R15A regulatory subunit fragments were unable to accelerate eIF2α dephosphorylation beyond that affected by a catalytic subunit alone, whether PP1 was purified from rabbit muscle or from bacteria. Furthermore, we did not observe Sephin1 or Guanabenz inhibition of eIF2α dephosphorylation by any PPP1R15A-containing holophosphatase.

(142 words)

Introduction

The integrated stress response (ISR) is a signal transduction pathway that couples diverse stressful conditions to the activation of a rectifying translational and transcriptional program that is implicated in biological processes ranging from memory formation to immunity and metabolism (reviewed in Ref. 5). The mammalian ISR and its yeast counterpart (the general control response) are initiated by the phosphorylation of the α subunit of translation initiation factor 2 (eIF2α) on serine 51[6,7] and its activity is terminated by eIF2α^P dephosphorylation.

Two related regulatory proteins, encoded in mammals by *PPP1R15A* and *PPP1R15B* (also known as GADD34 and CReP), direct the unspecific Protein Phosphatase 1 (PP1) to promote eIF2α^P dephosphorylation[8-11]. PPP1R15A and PPP1R15B form a complex with PP1 via a ~70 conserved amino acid region (PPP1R15A residues 555-624) located at their C-termini[2,9,12-14] (**Fig. 1a**). This conserved C-terminal region of either PPP1R15 regulatory subunit is sufficient to promote eIF2α^P dephosphorylation and to inactivate the ISR[2,8,9,14]. Indeed, Herpes viruses have exploited this activity and encode a small protein homologous to the C-terminus of PPP1R15 to reverse eIF2α phosphorylation, undoing a defensive strategy of infected cells[15].

Despite genetic evidence pointing to the sufficiency of the conserved C-terminal portion of PPP1R15 in reversing the eIF2α^P-dependent ISR *in vivo*[2,8,9], complexes formed *in vitro* between PPP1R15 regulatory subunit fragments and PP1 have been observed to unexpectedly lack specificity towards eIF2α^P [2]. Dephosphorylation of eIF2α^P is no faster by a complex of PPP1R15A-PP1 (or PPP1R15B-PP1) than by PP1 alone, showing that PP1R15A/B do not influence k_{cat} or K_m of PP1 towards the specific substrate eIF2α^P [2]. However, addition of G-actin to the binary complex selectively accelerates eIF2α^P dephosphorylation. G-actin binds directly to the C-terminus of PPP1R15 to form a ternary complex, whose affinity (K_d~10^{-8} M) matches

the EC_{50} of G-actin's stimulatory effect[2,4]. The *in vivo* relevance of G-actin to eIF2α^P dephosphorylation is attested to by the finding that actin sequestration in fibres (as F-actin) enfeebles eIF2α^P dephosphorylation, implying a role for factors that affect the actin cytoskeleton in ISR regulation[1].

The ability to dephosphorylate eIF2α^P is an essential function[16]. Nonetheless, inactivation of the *PPP1R15A* gene, which decelerates eIF2α^P dephosphorylation and prolongs the ISR and has proven protective in certain cellular and animal models of diseases associated with enhanced unfolded protein stress[17-20]. This has generated interest in targeting the PPP1R15A-containing holophosphatase for inhibition by small molecules (reviewed in Ref. 21), an endeavour that requires detailed knowledge of the enzymatic mode of action.

A recent report published in *Nature Structure and Molecular Biology*[3] challenged the need for G-actin as a co-factor in PPP1R15A-mediated eIF2α^P dephosphorylation. Instead, it was suggested that a binary complex assembled from PP1α and a fragment of PPP1R15A (PPP1R15A$^{325-636}$), encompassing both the C-terminal PP1-binding region and an N-terminal extension, dephosphorylates eIF2α^P faster than PP1 alone[3]. Importantly, dephosphorylation of eIF2α^P by this active binary complex was reported to be selectively inhibited by Guanabenz and Sephin1, two structurally-related small molecule proteostasis modifiers[22,23]. These findings contradict our observation that neither the non-selective PPP1R15A-PP1 binary complex, nor the eIF2α^P-selective PPP1R15A-PP1-G-actin ternary complex were susceptible to these inhibitors[4, 13].

To establish if these discrepant findings reflected differences in enzyme subunit preparations or experimental regimes, we set out to reproduce the experiments in ref. 3. Our findings, reported below, indicate that over a broad range of enzyme concentrations and time regimes, binary complexes comprised of preparations of native or recombinant PP1 with the PPP1R15A regulatory subunit construct used in

ref. 3 maintain stringent dependence on G-actin and are not measurably affected by the small molecule regulators Sephin1 or Guanabenz.

Results & Discussion

Native PP1 or bacterially-expressed PP1α require the presence of G-actin to promote PPP1R15A-regulated eIF2α^P dephosphorylation

PP1 produced in *E. coli* may differ in its enzymatic activity from PP1 purified from animal tissues, both in its substrate specificity and sensitivity to regulatory subunits (reviewed in ref. 24). To determine if the G-actin-dependence of PP1-PPP1R15A-mediated eIF2α^P dephosphorylation observed in our laboratory was a peculiarity of the bacterially-expressed PP1γ used[2,4], we purified the native catalytic subunit of PP1 from rabbit skeletal muscle (PP1^N), following an established protocol[25], and compared the two PP1 preparations. Native PP1 (PP1^N) is a mixture of PP1α, PP1β and PP1γ isoforms and gave rise to two prominent bands on SDS-PAGE (**Supplementary Fig.1a**, left panel). The mass spectra of tryptic peptides derived from the PP1^N sample was analysed by Maxquant with iBAQ (intensity based absolute quant) to estimate the relative contribution of PP1 and the major contaminating species, tropomyosin, and enable a comparison of the catalytic subunit content of PP1^N preparation with the bacterially-expressed PP1γ, which served as a reference.

Fig.1b shows that addition of either PPP1R15A$^{325-636}$ (lanes 5-8) or G-actin (lanes 13 & 14) did not stimulate eIF2α^P dephosphorylation by nanomolar concentrations of PP1^N. However, addition of both G-actin and PPP1R15A$^{325-636}$ (lanes 9-12) stimulated dephosphorylation 5-fold (**Fig.1b**), similar to the increase observed with bacterially expressed PP1γ (**Supplementary Fig.1b**)[2].

Residues 1-324 of PPP1R15A mediate membrane association[26], but are insoluble when expressed *in vitro*. Therefore, the experiments presented in **Fig.1b** used a PPP1R15A$^{325-636}$ fragment lacking the membrane-anchoring domain, which is soluble when expressed in *E. coli*. Importantly, this is the identical fragment of PPP1R15A

used in ref. 3. However, the location of the maltose binding protein (MBP)-tag, (which promotes solubility in biochemical experiments) differed between the two studies: C-terminal in **Fig. 1b** and N-terminal in ref. 3. Furthermore, PP1 purified from rabbit muscle is a mixture of α, β and γ isoforms, whereas PP1 used in ref. 3 was bacterially-expressed PP1α (an isoform reported to posses *in vivo* selectivity for PPP1R15A[10]), prepared by a method that promotes the native-like state of PP1[27]. To determine if these differences in the PPP1R15A construct or source of PP1 might account for the divergent observations, we generated N-terminally MBP-tagged PPP1R15A$^{325-636}$ expressed from the same pMAL-c5x-His bacterial expression plasmid and prepared PP1α using the stringent procedure followed in ref. 3 (**Supplementary Fig.1a**). However, in this system, aimed to closely reproduce the experiments reported in ref. 3, eIF2α^{P} dephosphorylation also exhibited a stringent requirement for both PPP1R15A and G-actin (**Fig.1c**).

A concentration-dependent stimulatory effect of PPP1R15A on eIF2α^{P} dephosphorylation by the three component holoenzyme (PP1, PP1R15A and G-actin) was observed with constructs tagged at either their N- or C-termini and with either native or bacterially-expressed PP1 (**Fig.2a-b**). The difference in EC_{50} values obtained for PPP1R15A$^{325-636}$-MPB with PP1^{N} (23 nM) or MBP-PPP1R15A$^{325-636}$ with PP1α (6 nM) may reflect the effect of the position of the MBP-tag, the contaminating tropomyosin (in PP1^{N}), or both. Importantly, the data agreed with a previously reported similar experiment in which PPP1R15A$^{325-636}$ and bacterially-expressed PP1γ were used (10 nM, ref. 4, figure 8A therein).

G-actin also exerted a saturable concentration-dependent stimulatory effect on the activity of a three-component holophosphatase constituted with native PP1^{N} **(Fig.2c)**. The EC_{50} for G-actin with PP1^{N} (24 nM) was similar to that previously observed using bacterially-expressed PP1γ (13 nM, ref. 4, figure 2C therein). Hence, despite small variations in the estimated EC_{50} values for PP1R15A or G-actin, all combinations of

catalytic and regulatory subunits tested showed consistent PPP1R15A and G-actin concentration dependent enzymatic activity. These experiments, conducted in a concentration range (nanomolar catalytic subunit and micromolar substrate) similar to that employed in ref. 3, indicate that neither the source of PP1 nor the position of the tag in PPP1R15A are likely to account for the G-actin independent ability of PPP1R15A to stimulate eIF2α^{P} dephosphorylation reported in that study.

Lengthy incubation of the enzymatic reactions does not uncover PPP1R15A's ability to promote G-actin-independent eIF2α^{P} dephosphorylation.

Upon inhibition of the phosphorylating kinase, the eIF2α^{P} signal decays with a $T_{1/2}$ of <10 minutes (with no change in the total eIF2α content) in both cultured mouse fibroblasts (Ref. 1, figure 6 therein) and Chinese Hamster Ovary cells (Ref. 4, figure 10 therein). Despite the rapid *in vivo* kinetics of the dephosphorylation reaction, all experiments in ref. 3 were conducted using a long incubation of 16 hours at 30˚C. In the absence of other components PP1α is markedly unstable at 30˚C, losing about half of its activity by 1 hour and all detectable activity by 3 hours (**Supplementary Fig.2a-b**). Thus a stabilizing effect of a PP1 binding co-factor might have accounted for the apparent G-actin-independent stimulatory effect of MBP-PPP1R1A$^{325-636}$ on PP1α-mediated eIF2α^{P} dephosphorylation observed over the lengthy incubations of ref. 3. However, over a range of PP1 concentrations (0.2-200 nM), the presence of MBP-PPP1R15$^{325-636}$ (at a constant concentration of 50 nM, indicated in ref. 3) failed to stimulate eIF2α^{P} dephosphorylation, whether PP1^{N} (**Fig.3a**) or PP1α (**Fig.3b**) were used.

To further promote comparability of the experimental conditions used here to those of ref. 3, we used PhosTag gels from the same commercial source (Alpha laboratories), and confirmed that the proteins used in our experiments exhibited the expected mobility for these gels (**Supplementary Fig. 2c**). Despite our best efforts we have

been unable to reproduce the stimulatory effect of MBP-PPP1R15A$^{325-636}$ on eIF2α^{P} dephosphorylation.

Substrate recruitment by the PPP1R15A$^{325-512}$ region plays a secondary role in the kinetics of eIF2α^{P} dephosphorylation and its reported disruption is unlikely to account for Sephin1's activity.

PPP1R15A interacts directly with eIF2α, both in cells[13] and *in vitro*[3]. This interaction mapped to PPP1R15A residues 325-512; N-terminal to PPP1R15A's PP1-binding domain (**Fig.1a**) and was proposed to play an important role in PPP1R15A's ability to promote eIF2α^{P} dephosphorylation[3]. However, in the presence of G-actin, PPP1R15A$^{325-636}$ and PPP1R15A$^{533-624}$ stimulated eIF2α^{P} dephosphorylation similarly, with either with PP1^{N} (compare **Fig.4a** and **Fig.2a** here) or with PP1γ (compare Figure 8A and Figure 2B in Ref. 4). These findings suggest that the PP1R15A PP1-binding region, together with G-actin, are sufficient to promote eIF2α^{P} dephosphorylation and dominate its kinetics *in vitro*.

Despite this evidence against an essential regulatory role for substrate engagement by PPP1R15A$^{325-533}$, it remained possible that other compensatory features that diverge between the different regulatory subunit constructs might equalize their activity, masking an important effect of the PPP1R15A$^{325-512}$ region on enzyme kinetics. Therefore, we measured the ability of MBP-PPP1R15A$^{325-512}$ to compete with MBP-PPP1R15A$^{325-636}$-mediated (G-actin-dependent) eIF2α^{P} dephosphorylation using PP1α as the catalytic subunit. Minimal inhibition of the dephosphorylation reaction was observed at competitor concentrations of up to 8 μM (**Fig.4b**), which is a >300-fold excess over the MBP-PPP1R15A$^{325-636}$ regulatory subunit (present in the reaction at 24 nM), and a concentration of 18-fold above the K_d of the interaction between MBP-PPP1R15A$^{325-512}$ and eIF2α^{P} (measured in ref. 3, figure 3b therein). These data suggest that substrate recruitment by the N-terminal extension of PPP1R15A plays a secondary role in the kinetics of the dephosphorylation reaction

and that the role of Sephin1 and Guanabenz in disrupting that interaction (reported in ref. 3) is unlikely to make an important contribution to their pharmacological activity.

These conclusions not withstanding, we further considered that the particular proteins used in ref. 3 (recombinant PP1α, and N-terminally-MBP-tagged PPP1R15A$^{325-636}$) might have accounted for the observed Sephin1 and Guanabenz sensitivity of the dephosphorylation reaction in that study. However, under conditions in which eIF2α^{P} dephosphorylation is dependent on the concentration of both PP1α and MBP-PPP1R15A$^{325-636}$ (both prepared as in ref. 3), we were unable to observe an inhibitory effect of Sephin1 or Guanabenz at a concentration of 100 μM (**Fig.5**), which exceeds by two-fold that required for a proteostatic effect in cultured cells[4,23].

Conclusions:

The new experiments presented here cover a range of conditions with realistic concentrations and time regimes. Our observations were made with two different PPP1R15A preparations and three different PP1 preparations, all of which reinforce the requirement for G-actin as an additional co-factor in enabling PPP1R15A to stimulate eIF2α^{P} dephosphorylation *in vitro*. Our experiments also cast uncertainty on a role for PPP1R15A residues 325-533 in promoting the dephosphorylation reaction and the role of Sephin1 and Guanabenz as inhibitors of PPP1R15A-mediated eIF2α^{P} dephosphorylation.

As such the results presented here are in keeping with previous observations that G-actin has an essential role in promoting eIF2α^{P} dephosphorylation both *in vitro* and *in vivo* (ref. 1, Figure 6 therein). They are also in accordance with the observations that Sephin1 and Guanabenz have no measurable effect on the rate of eIF2α^{P} dephosphorylation in cells with PPP1R15A as their only known eIF2α^{P}-directed regulatory subunit and with the observation that Sephin1's effect on stress-induced

gene expression is also observed in PPP1R15A deficient cells as well as in cells containing a non-phosphorylatable eIF2α[4].

Author Contributions

ACC: Conceived the study, co-designed and conducted the experiments, interpreted the results, created the figures and co-wrote the paper

ZC: Co-designed the experiments, assisted with the preparation of PP1 from rabbit muscle, interpreted the results, edited the manuscript.

MC: Expressed and purified PP1α from *E. coli*, interpreted the results, edited the manuscript.

WP: Oversaw the expression and purification of PP1α from *E. coli*, interpreted the results, edited the manuscript.

MB: Co-designed the experiments, oversaw the purification of PP1 from rabbit muscle, interpreted the results, edited the manuscript.

DR: Conceived the study. Co-designed the experiments, interpreted the results, and co-wrote the paper

Acknowledgements

We thank Alison Schuldt and members of the Ron laboratory for their comments on the manuscript. Stefan Marciniak and Joe Chambers for useful ideas for experiments and comments on the manuscript. Robin Antropus for mass spectrometry analysis support. Supported by a Wellcome Trust Principal Research Fellowship to D.R. (Wellcome 200848/Z/16/Z) and a Wellcome Trust Strategic Award to the Cambridge Institute for Medical Research (Wellcome 100140). M.B. was supported by a Flemish Concerted Research Action (GOA15/016). W.P. was supported by National Institute of Health R01 NS091336 and the American Diabetes Association Pathway to Stop Diabetes Grant 1-14-ACN-31. Z.C. is a PhD fellow of the Fund for Scientific Research - Flanders.

References

1. Chambers, J.E. et al. Actin dynamics tune the integrated stress response by regulating eukaryotic initiation factor 2alpha dephosphorylation. *Elife* **4**(2015).
2. Chen, R. et al. G-actin provides substrate-specificity to eukaryotic initiation factor 2alpha holophosphatases. *Elife* **4**, e04871 (2015).
3. Carrara, M., Sigurdardottir, A. & Bertolotti, A. Decoding the selectivity of eIF2alpha holophosphatases and PPP1R15A inhibitors. *Nat Struct Mol Biol* **24**, 708-716 (2017).
4. Crespillo-Casado, A., Chambers, J.E., Fischer, P.M., Marciniak, S.J. & Ron, D. PPP1R15A-mediated dephosphorylation of eIF2alpha is unaffected by Sephin1 or Guanabenz. *Elife* **6**(2017).
5. Pakos-Zebrucka, K. et al. The integrated stress response. *EMBO Rep* **17**, 1374-1395 (2016).
6. Dever, T.E. et al. Phosphorylation of initiation factor 2 alpha by protein kinase GCN2 mediates gene-specific translational control of GCN4 in yeast. *Cell* **68**, 585-96 (1992).
7. Harding, H.P. et al. An integrated stress response regulates amino acid metabolism and resistance to oxidative stress. *Mol Cell* **11**, 619-33 (2003).
8. Jousse, C. et al. Inhibition of a constitutive translation initiation factor 2alpha phosphatase, CReP, promotes survival of stressed cells. *J Cell Biol* **163**, 767-75 (2003).
9. Novoa, I., Zeng, H., Harding, H. & Ron, D. Feedback inhibition of the unfolded protein response by GADD34-mediated dephosphorylation of eIF2a. *J Cell Biol* **153**, 1011-1022 (2001).
10. Brush, M.H., Weiser, D.C. & Shenolikar, S. Growth arrest and DNA damage-inducible protein GADD34 targets protein phosphatase 1 alpha to the endoplasmic reticulum and promotes dephosphorylation of the alpha subunit of eukaryotic translation initiation factor 2. *Mol Cell Biol* **23**, 1292-303 (2003).
11. Ma, Y. & Hendershot, L.M. Delineation of a Negative Feedback Regulatory Loop That Controls Protein Translation during Endoplasmic Reticulum Stress. *J Biol Chem* **278**, 34864-73 (2003).
12. Connor, J.H., Weiser, D.C., Li, S., Hallenbeck, J.M. & Shenolikar, S. Growth arrest and dna damage-inducible protein gadd34 assembles a novel signaling complex containing protein phosphatase 1 and inhibitor 1. *Mol Cell Biol* **21**, 6841-50. (2001).
13. Choy, M.S. et al. Structural and Functional Analysis of the GADD34:PP1 eIF2alpha Phosphatase. *Cell Rep* **11**, 1885-91 (2015).
14. Malzer, E. et al. Coordinate regulation of eIF2alpha phosphorylation by PPP1R15 and GCN2 is required during Drosophila development. *J Cell Sci* **126**, 1406-15 (2013).
15. He, B., Gross, M. & Roizman, B. The gamma134.5 protein of herpes simplex virus 1 has the structural and functional attributes of a protein phosphatase 1 regulatory subunit and is present in a high molecular weight complex with the enzyme in infected cells. *J Biol Chem* **273**, 20737-43 (1998).
16. Harding, H.P. et al. Ppp1r15 gene knockout reveals an essential role for translation initiation factor 2 alpha (eIF2alpha) dephosphorylation in mammalian development. *Proc Natl Acad Sci USA* **106**, 1832-7 (2009).
17. Marciniak, S.J. et al. CHOP induces death by promoting protein synthesis and oxidation in the stressed endoplasmic reticulum. *Genes and Development* **18**, 3066-3077 (2004).

18. Lin, W. et al. Enhanced Integrated Stress Response Promotes Myelinating Oligodendrocyte Survival in Response to Interferon-{gamma}. *Am J Pathol* **173**, 1508-17 (2008).
19. D'Antonio, M. et al. Resetting translational homeostasis restores myelination in Charcot-Marie-Tooth disease type 1B mice. *J Exp Med* **210**, 821-38 (2013).
20. Wang, L., Popko, B. & Roos, R.P. An enhanced integrated stress response ameliorates mutant SOD1-induced ALS. *Hum Mol Genet* **23**, 2629-38 (2014).
21. Schneider, K. & Bertolotti, A. Surviving protein quality control catastrophes--from cells to organisms. *J Cell Sci* **128**, 3861-9 (2015).
22. Tsaytler, P., Harding, H.P., Ron, D. & Bertolotti, A. Selective inhibition of a regulatory subunit of protein phosphatase 1 restores proteostasis. *Science* **332**, 91-4 (2011).
23. Das, I. et al. Preventing proteostasis diseases by selective inhibition of a phosphatase regulatory subunit. *Science* **348**, 239-42 (2015).
24. Peti, W., Nairn, A.C. & Page, R. Structural basis for protein phosphatase 1 regulation and specificity. *FEBS J* **280**, 596-611 (2013).
25. DeGuzman, A. & Lee, E.Y. Preparation of low-molecular-weight forms of rabbit muscle protein phosphatase. *Methods Enzymol* **159**, 356-68 (1988).
26. Zhou, W., Brush, M.H., Choy, M.S. & Shenolikar, S. Association with endoplasmic reticulum promotes proteasomal degradation of GADD34 protein. *J Biol Chem* **286**, 21687-96 (2011).
27. Kelker, M.S., Page, R. & Peti, W. Crystal structures of protein phosphatase-1 bound to nodularin-R and tautomycin: a novel scaffold for structure-based drug design of serine/threonine phosphatase inhibitors. *J Mol Biol* **385**, 11-21 (2009).
28. Pardee, J.D. & Spudich, J.A. Purification of muscle actin. *Methods Enzymol* **85 Pt B**, 164-81 (1982).
29. Choy, M.S. et al. Understanding the antagonism of retinoblastoma protein dephosphorylation by PNUTS provides insights into the PP1 regulatory code. *Proc Natl Acad Sci U S A* **111**, 4097-102 (2014).

Materials and methods

Protein expression and purification

The plasmids used to express protein in *E. coli* are presented in **Supplementary Table 1**.

PPP1R15A$^{325-636}$-MBP and PPP1R15A$^{533-624}$-MBP were purified according to[4]. Briefly, proteins were expressed in *E. Coli* BL21 (C3013) as N-terminally-tagged glutathione S-transferase fusion protein and purified by tandem affinity chromatography. First by binding to a glutathione sepharose 4B resin, elution with glutathione, followed by an overnight cleavage with Tobacco Etch Virus (TEV) protease (to remove the GST tag), binding to amylose beads and elution in maltose-containing buffer.

MBP-PPP1R15A$^{325-636}$ and **MBP-PPP1R15A$^{325-512}$**: *E. coli* BL21 (C3013) were transformed with the ampicillin-resistance pMAL-c5x-His vector (New England Biolabs, Cat. No. N8114) containing PPP1R15A$^{325-636}$ and were selected in LB agar plates supplemented with 100 μg/ml ampicillin. A single colony was picked to grow overnight in 5 mL starter culture that served to inoculate 2 L of LB media (all supplemented with 100 μg/mL ampicillin), which was kept at 37°C. At OD_{600}=0.6-0.8 protein expression was induced using 1 mM Isopropyl β-D-1-thiogalactopyranoside (IPTG) at 18°C for 20 hours. Bacteria were pelleted and resuspended in ice-cold His6 Lysis Buffer containing 50 mM Tris pH 7.4, 500 mM NaCl, 1 mM $MgCl_2$, 1 mM tris (2-carboxyethyl)phosphine (TCEP), 100 μM phenylmethylsulfonyl fluoride (PMSF), 20 mTIU/ml aprotinin, 2 μM leupeptin, and 2 μg/ml pepstatin 20 mM imidazole and 10% glycerol. Bacterial suspensions were lysed using an Emulsi-Flex-C3 homogenizer (Avestin, Inc, Ottawa, Ontario) and clarified in a JA-25.50 rotor (Beckman Coulter) at 33,000 x g for 30 min at 4°C. Pre-equilibrated Ni-NTA beads (Qiagen, Cat. No. 30230,) were incubated with the samples for 2 hours at 4°C.

Proteins were eluted in 2 mL of Imidazole Elution Buffer (50 mM Tris, pH 8, 100 mM NaCl, 500 mM Imidazole, 10% glycerol) and incubated with amylose beads (New England Biolabs, Cat No. E8021S) pre-equilibrated with Lysis Buffer (His6 Lysis Buffer without imidazole) for 2 hours at 4°C. The amylose beads were batch-washed using 25 bed volumes of Lysis Buffer and proteins were eluted with Amylose Elution Buffer (Lysis Buffer + 10 mM maltose). MBP-R15A$^{325-512}$ purification required an additional buffer exchange step (into Lysis Buffer) using Centri pure P1 gel filtration columns (EMP Biotech, Cat. No. CP-0110) to eliminate maltose that appeared to interfere with the dephosphorylation reactions when present at high concentrations.

eIF2α^{P}: The N-terminal fragment of human eIF2α (1-185, with three solubilizing mutations) was purified from bacteria and phosphorylated in vitro using the kinase domain of PERK[2]

G-actin was purified from rabbit muscle according to ref. 28 as modified in ref. 2.

PP1γ (7-300) was purified according to ref. 4.

PP1α (7-330) was purified from BL21 *E. coli* according to ref. 27 and 29

PP1^{N} was purified from rabbit muscle according to ref. 25

In vitro dephosphorylation reactions

Reactions were performed at a final volume of 20 μL consisting of 5 μL of 4X solution of each component: PP1, PPP1R15A, G-actin and eIF2α^{P} (or their respective buffers). A 10X assay buffer (500 mM Tris pH 7.4, 1 M NaCl, 1 mM EDTA, 0.1% Triton X-100, 10 mM $MgCl_2$) was diluted 1:10, supplemented with 1 mM DTT and used to create working solutions of PP1, PPP1R15A and eIF2α^{P} at the desired concentrations. G-actin working solutions were created using G-buffer (2 mM Tris at pH 8, 0.2 mM ATP, 0.5 mM DTT and 0.1 mM $CaCl_2$). Holoenzyme components (PP1, PPP1R15A and G-actin) were combined first and substrate (eIF2α^{P}) was

added later to initiate the reactions, which were conducted under shaking at 500 rpm and at 30˚C for the specified time.

The stability test of PP1α (**Supplementary Fig.2**) was performed by preparing a fresh 240 nM solution of PP1α in the assay buffer described above. Separate aliquots were pre-incubated either at 30˚C or on ice for the specified times (30 minutes to 7 hours, see schema in **Supplementary Fig.2a**). At termination of the preincubation, 5 μL of these pre-incubated solutions were added into 20 μL dephosphorylation reactions as described above.

Reactions performed in **Fig.5**, included a 15 minutes pre-incubation of the enzymatic components at room temperature (before addition of substrate). Solutions of 4x PP1 (96 nM) were supplemented with either 400 μM Sephin1 (Enamine, Cat. No. EN300-195090) or Guanabenz (Sigma-Aldrich, Cat. No. D6270), 320 nM Tautomycin (Calbiochem, Cat. No. 5805551) or DMSO. Five microliters of these solutions were incubated with 5 μL PPP1R15A and 5 μL G-actin for 15 minutes before adding eIF2α^P substrate to initiate the reaction in a final volume of 20 μL.

Reactions were terminated by addition of 10 μL of 3X Laemmli buffer supplemented with 100 mM DTT and heating the samples for 5 minutes at 70˚C. A third (10 μL) of the final volume was resolved in 12.5% PhosTag SDS gels (Wako, Cat. No. NARD AAL-107) or 15% precast Phostag SDS-PAGE gels (Alpha laboratories, Cat. No. 2614190) at 200 V for 1 hour. Gels were stained with Coomassie Instant Blue and imaged on an Odyssey imager.

ImageJ was used for band quantification and GraphPad Prism v7 was used to fit data using the '[Agonist] vs. response (three parameters)' analysis function.

Supplementary Table 2 lists the number of times each experiment was performed.

Figure legends

Figure 1. PPP1R15A accelerates eIF2α^P dephosphorylation by either PP1^N or PP1α only in the presence of G-actin

a. Cartoon representation of human PPP1R15A protein (1-674). Key residues used for truncated versions of the proteins in this study are annotated. The proline, glutmate, serine and threonine-rich (PEST) repeats are highlighted as are the PP1 and G-actin binding sites in the conserved C-terminal region**.**

b. Upper panel. Coomassie-stained PhosTag-SDS-PAGE containing resolved samples of dephosphorylation reactions (30 minutes at 30˚C) in which 2 μM eIF2α^P was dephosphorylated by PP1^N purified from rabbit skeletal muscle in the presence or absence of PPP1R15A$^{325-636}$-MBP (50 nM) and/or G-actin (400 nM). The position of the various protein species is indicated. eIF2α^P and eIF2α^0 refer to the phosphorylated and non-phosphorylated form of the bacterially-expressed N-terminal domain (residues 1-185) of eIF2α, respectively. Note that both G-actin and PP1^N preparation gave rise to two bands: a major full-length species and minor degradation product, in the case of G-actin, and a PP1 and tropomyosin band in the case of PP1^N (see also **supplementary Fig. 1**). Shown is a representative experiment of four independent repetitions performed.

Lower panel. Plot of the rate of eIF2α^P dephosphorylation as a function of the concentration of PP1^N in the experiment above.

c. As in "**b**" but using bacterially-expressed PP1α as the catalytic subunit (96, 48, 24 or 12 nM), MBP-PPP1R15A$^{325-636}$ (50 nM) and G-actin (400 nM). The assays were performed during 20 minutes at 30˚C. Shown is a representative experiment of three independent repetitions performed.

Figure 2. The source of catalytic subunit does not affect the kinetics of PPP1R15A and G-actin-mediated stimulation of eIF2α^P dephosphorylation

a. Upper panel. Coomassie-stained PhosTag-SDS-PAGE of dephosphorylation reactions (30 minutes at 30˚C), in which 2 μM eIF2α^P was dephosphorylated by PP1^N (20 nM) in presence of G-actin (400 nM) and increasing concentrations of PPP1R15A$^{325-636}$-MBP (0-100 nM). Shown is a representative experiment of three independent experiments performed.

Lower panel. Plot of the rate of dephosphorylation of eIF2α^P as a function of PPP1R15A$^{325-636}$-MBP concentration, from the three experiments performed. The EC_{50} was calculated using the "[Agonist] vs. response (three parameters)" function in GraphPad Prism v7.

b. As in "**a**" but using bacterially-expressed PP1α (24 nM) and increasing concentrations of MBP-PPP1R15A$^{325-636}$ (0-100 nM) in reactions performed over 20 minutes at 30˚C. Shown is a representative experiment of three independent experiments performed.

c. As in "**a**" but with fixed concentrations of PP1^N (20 nM) and PPP1R15A$^{325-636}$-MBP (50 nM) and varying the concentrations of G-actin (1-2000 nM). Shown is a representative experiment of three independent experiments performed.

Figure 3. In the absence of G-actin, PPP1R15A is unable to stimulate dephosphorylation of eIF2α^P (despite an extended incubation of 16h).

a. Upper panel. Coomassie-stained PhosTag-SDS-PAGE (from Alpha laboratories) containing dephosphorylation reactions (16 hours at 30˚C) in which 2 μM eIF2α^P was dephosphorylated by the indicated concentration of $PP1^N$ in the presence or absence of $PPP1R15A^{325-636}$-MBP (50 nM). Quantification of percentage of dephosphorylation (%dP) is shown below the image. Shown is a representative experiment of two independent repetitions performed.

Lower panel. Plot of the rate of dephosphorylation of eIF2α^P as a function of $PP1^N$ concentration. Data was obtained by quantification of bands of image shown above.

b. As in "**a**" but using PP1α as the source of catalytic subunit and MBP-$PPP1R15A^{325-636}$ (50 nM) as the regulatory subunit. Shown is a representative experiment of two independent repetitions performed.

Figure 4. The C-terminal portion of PPP1R15A is sufficient to promote eIF2α^P dephosphorylation.

a. Upper panel. Coomassie-stained PhosTag-SDS-PAGE containing resolved samples from dephosphorylation reactions (30 minutes at 30˚C) in which 2 μM eIF2α^P was dephosphorylated by PP1^N (20 nM) in the presence of G-actin (400 nM) and increasing concentrations of PPP1R15A$^{533-624}$-MBP (0-100 nM) . Shown is a representative experiment of three independent repetitions performed.

Lower panel. Plot of the rate of dephosphorylation of eIF2α^P as a function of PPP1R15A$^{533-624}$-MBP concentration, from the three experiments performed. The EC_{50} was calculated using the "[Agonist] vs. response (three parameters)" function in GraphPad Prism v7.

b. As in "**a**" but using PP1α (24 nM) in presence of MBP-PPP1R15A$^{325-636}$ (24 nM), G-actin (400 nM) and increasing concentrations of MBP-PPP1R15A$^{325-512}$ as a competitor (0-8 μM). The assays were performed during 20 minutes at 30˚C. Lane 8, loaded with only MBP-PPP1R15A$^{325-512}$ shows the absence of a species co-migrating with eIF2α^0 (which might otherwise obscure an inhibitory effect on dephosphorylation). Lanes 9 and 10 control for the dependence of enzymatic activity on PPP1R15A and G-actin in this experiment. Quantification of percentage of dephosphorylation (%dP) is shown below the image. Shown is a representative experiment of two independent repetitions performed.

Figure 5. Sephin1 does not interfere with eIF2α^P dephosphorylation

a. Coomassie-stained PhosTag-SDS-PAGE containing resolved samples from dephosphorylation reactions (20 minutes, 30˚C) in which 2 μM eIF2α^P was dephosphorylated by PP1α (24 nM) in presence or absence of MBP-PPP1R15A$^{325-636}$ (60 nM) and/or G-actin (400 nM). The components were pre-incubated as specified with either Sephin1 (100 μM), Tautomycin (80 nM) or DMSO (vehicle) for 15 minutes at room temperature before being added to the reaction. The bottom panel shows a long exposure of the relevant section of the image above corresponding to the phosphorylated and non-phosphorylated forms of eIF2α. Quantification of percentage of dephosphorylation (%dP) is shown below the image. Shown is a representative experiment of three independent experiments performed.

b. As in "**a**" but with Guanabenz (GBZ). Shown is a representative experiment of two independent experiments performed.

Supplementary Figure 1. Analysis of the purity of the different sources of PP1.

a. Coomassie-stained SDS-PAGE gels in which different amounts of PP1 sample have been resolved. The $PP1^N$ preparation gave rise to two bands: a PP1 and tropomyosin band. The PP1γ preparation contained some free Glutathione S Transferase (GST) and GST-PP1 fusion protein from the purification steps, as well as other minor contaminants (*). The PP1 concentration in the different preparations is shown below the panels, calculated using PP1γ as a reference.

b. Coomassie-stained PhosTag-SDS-PAGE containing resolved samples from dephosphorylation reactions (as in Fig. 1a and 1b) in which 2 μM $eIF2\alpha^P$ was dephosphorylated using bacterially-expressed PP1γ (24 nM) in presence or absence of $MBP\text{-}PPP1R15A^{325\text{-}636}$ (50 nM), $MBP\text{-}PPP1R15A^{325\text{-}512}$ (50 nM) and/or G-actin (400 nM) for 20 minutes at 30˚C. Quantification of percentage of dephosphorylation (%dP) is shown below the image.

Supplementary Figure 2. PP1α is an unstable enzyme.

a. Schema of the experiment. Samples of PP1 (at 240 nM) were pre-incubated for the indicated period of time, either on ice, or at 30˚C, before being diluted into a eIF2α^P dephosphorylation reaction.

b. Upper panel. Coomassie-stained PhosTag-SDS-PAGE containing samples from dephosphorylation reactions (20 minutes at 30˚C) in which 2 μM eIF2α^P was dephosphorylated by the pre-incubated PP1α (60 nM) in presence of MBP-PPP1R15A$^{325-636}$ (60 nM) and G-actin (400 nM).

Lower panel. Plot of the rate of dephosphorylation of eIF2α^P as a function of pre-incubation time of PP1α catalytic subunit. Data was obtained by quantification of bands of image shown above.

c. Coomassie-stained 15% PhosTag-SDS-PAGE (from Alpha Laboratories) containing specified amounts (in nanograms) of PP1α, MBP-PPP1R15A$^{325-636}$, eIF2α^P and eIF2α^0. This gel presents the mobility of eIF2α^0, eIF2α^P, MBP-PPP1R15A$^{325-636}$ and PP1α when added as single components to each lane at quantities corresponding to the content of a dephosphorylation reaction conducted at concentrations of 5 μM, 2 μM, 50 nM and 200 nM, respectively.

Figure 1

a

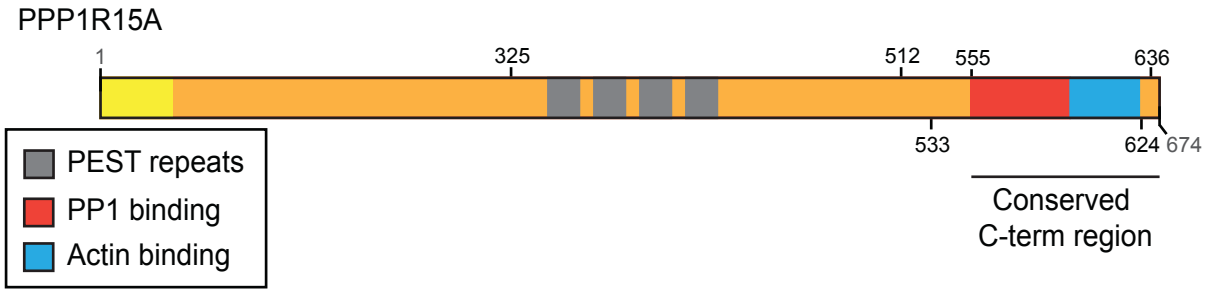
PPP1R15A
1
325
512
555
636
533
624
674
PEST repeats
PP1 binding
Actin binding
Conserved
C-term region

b

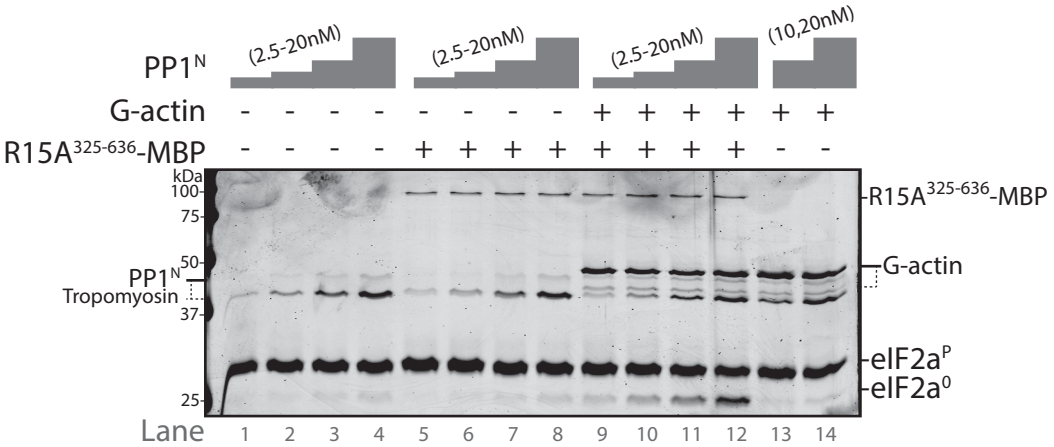
PP1N
(2.5-20nM)
(2.5-20nM)
(2.5-20nM)
(10,20nM)
G-actin
R15A325-636-MBP
kDa
100
75
50
37
25
PP1N
Tropomyosin
R15A325-636-MBP
G-actin
eIF2aP
eIF2a0
Lane
1 2 3 4 5 6 7 8 9 10 11 12 13 14

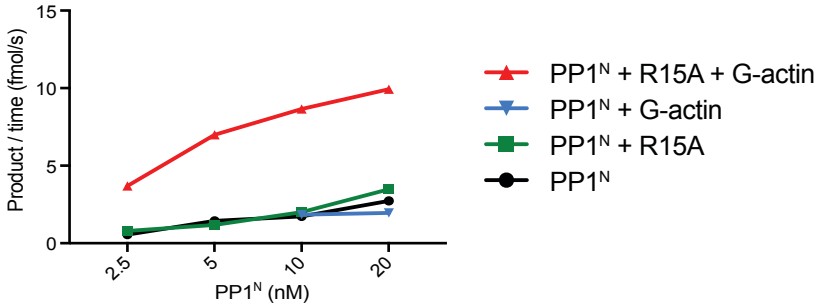
Product / time (fmol/s)
15
10
5
0
2.5
5
10
20
PP1N (nM)
PP1N + R15A + G-actin
PP1N + G-actin
PP1N + R15A
PP1N

c

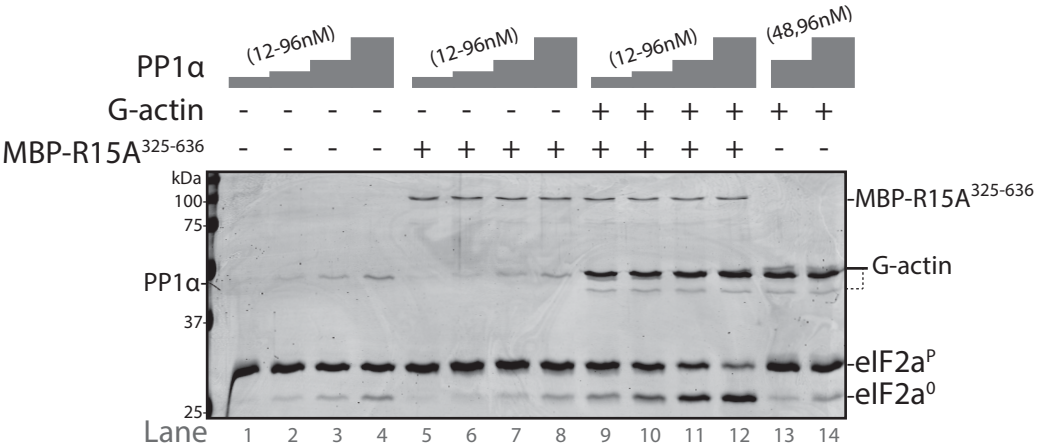
PP1α
(12-96nM)
(12-96nM)
(12-96nM)
(48,96nM)
G-actin
MBP-R15A325-636
kDa
100
75
37
25
PP1α
MBP-R15A325-636
G-actin
eIF2aP
eIF2a0
Lane
1 2 3 4 5 6 7 8 9 10 11 12 13 14

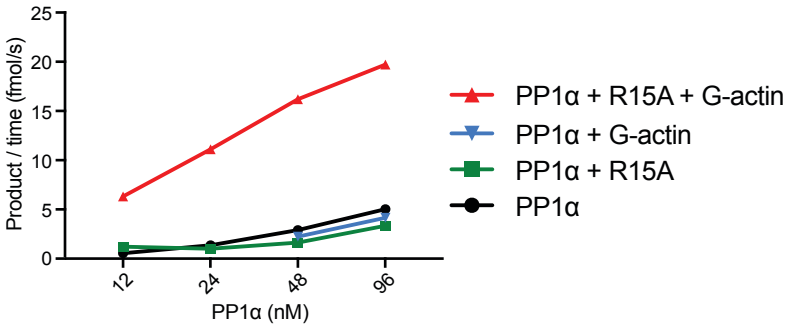
Product / time (fmol/s)
25
20
15
10
5
0
12
24
48
96
PP1α (nM)
PP1α + R15A + G-actin
PP1α + G-actin
PP1α + R15A
PP1α

Figure 2

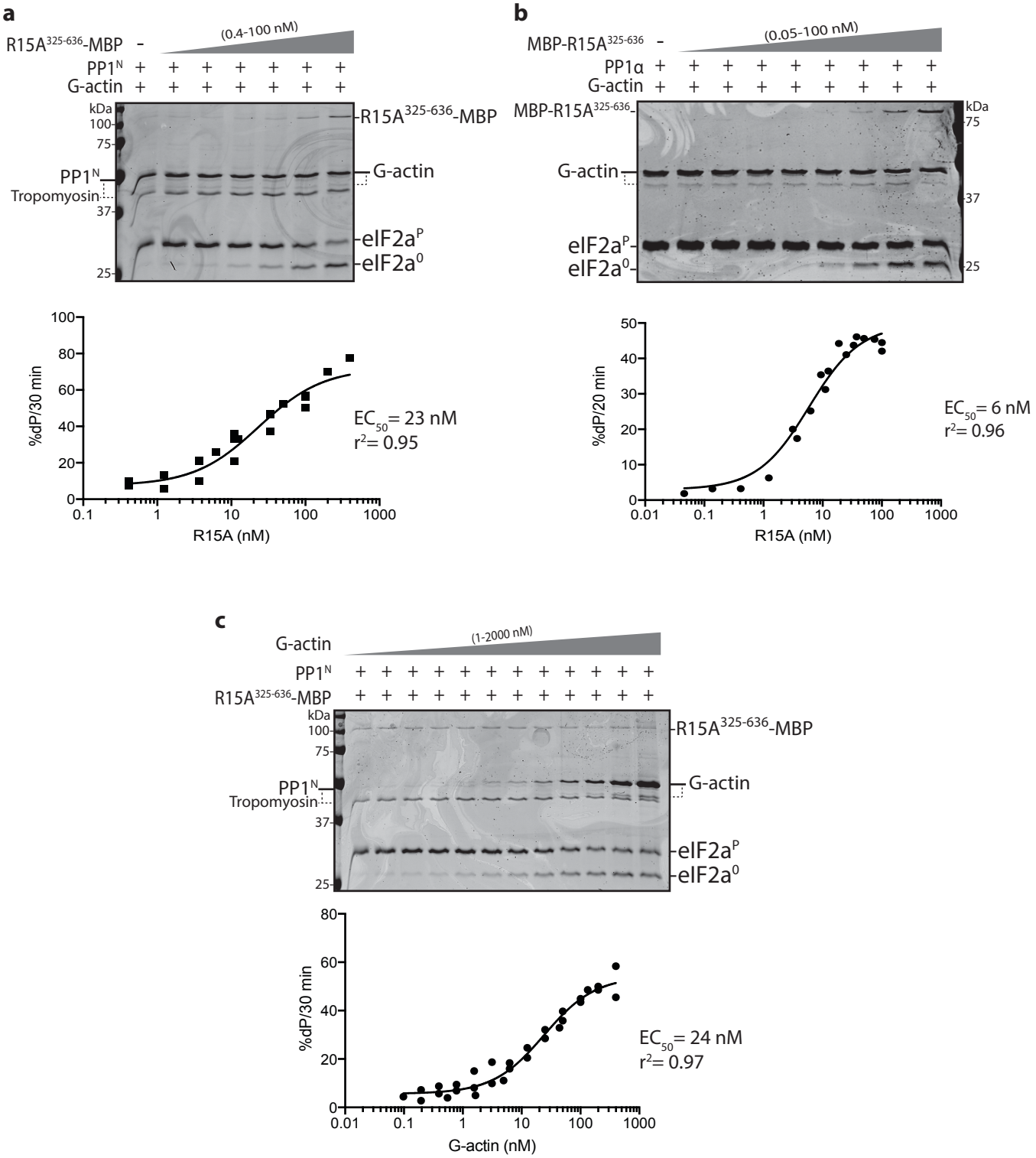
a
R15A325-636-MBP
(0.4-100 nM)
PP1N
G-actin
kDa
100
75
37
25
PP1N
Tropomyosin
R15A325-636-MBP
G-actin
eIF2aP
eIF2a0
%dP/30 min
EC50= 23 nM
r2= 0.95
R15A (nM)
b
MBP-R15A325-636
(0.05-100 nM)
PP1α
G-actin
MBP-R15A325-636
G-actin
eIF2aP
eIF2a0
kDa
75
37
25
%dP/20 min
EC50= 6 nM
r2= 0.96
R15A (nM)
c
G-actin
(1-2000 nM)
PP1N
R15A325-636-MBP
kDa
100
75
37
25
PP1N
Tropomyosin
R15A325-636-MBP
G-actin
eIF2aP
eIF2a0
%dP/30 min
EC50= 24 nM
r2= 0.97
G-actin (nM)

Figure 3

a

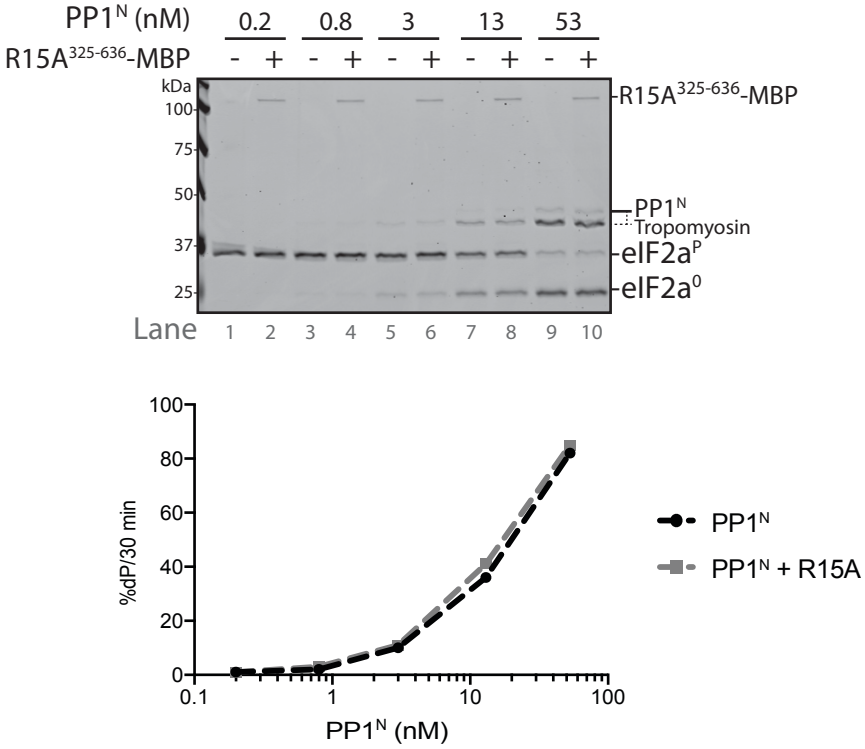
PP1N (nM)
0.2
0.8
3
13
53
R15A325-636-MBP
- + - + - + - + - +
kDa
100
75
50
37
25
R15A325-636-MBP
PP1N
Tropomyosin
eIF2aP
eIF2a0
Lane 1 2 3 4 5 6 7 8 9 10
%dP/30 min
PP1N
PP1N + R15A
PP1N (nM)

b

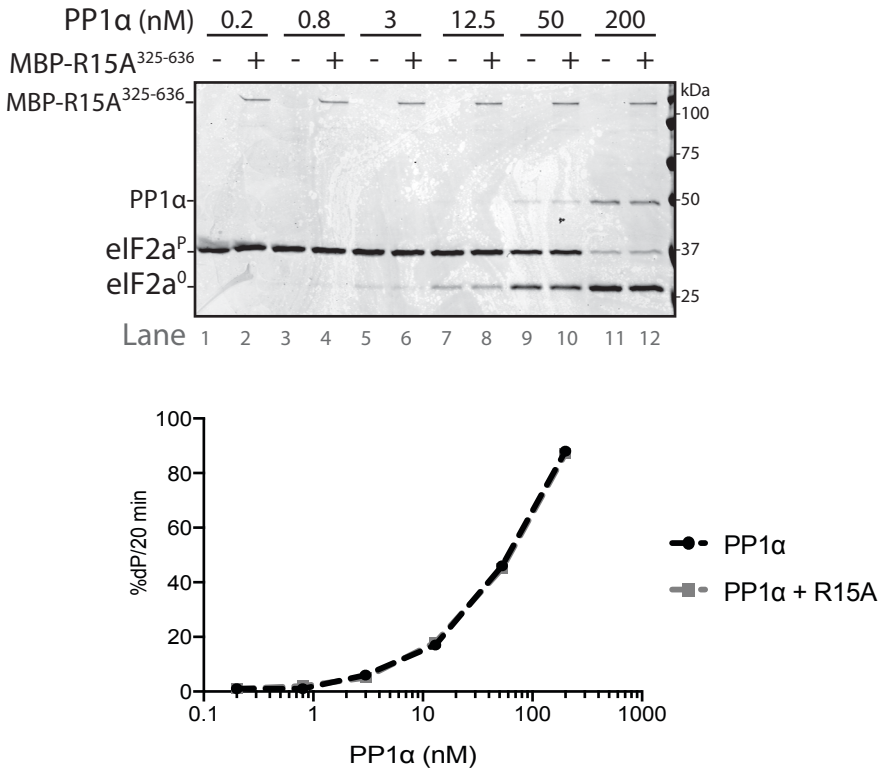
PP1α (nM)
0.2
0.8
3
12.5
50
200
MBP-R15A325-636
- + - + - + - + - + - +
MBP-R15A325-636
kDa
100
75
50
37
25
PP1α
eIF2aP
eIF2a0
Lane 1 2 3 4 5 6 7 8 9 10 11 12
%dP/20 min
PP1α
PP1α + R15A
PP1α (nM)

Figure 4

a

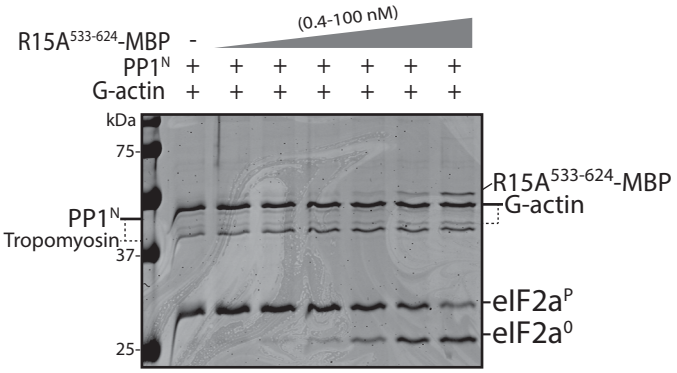
R15A533-624-MBP
(0.4-100 nM)
PP1N
G-actin
kDa
75
37
25
PP1N
Tropomyosin
R15A533-624-MBP
G-actin
eIF2aP
eIF2a0

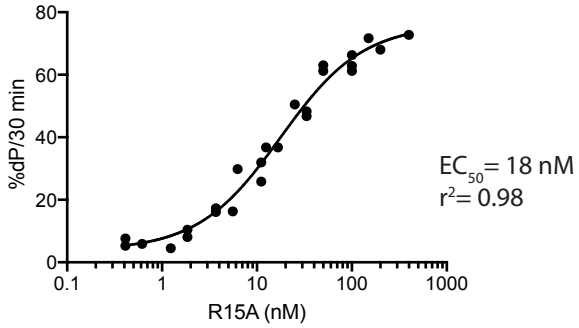
%dP/30 min
R15A (nM)
EC50= 18 nM
r2= 0.98

b

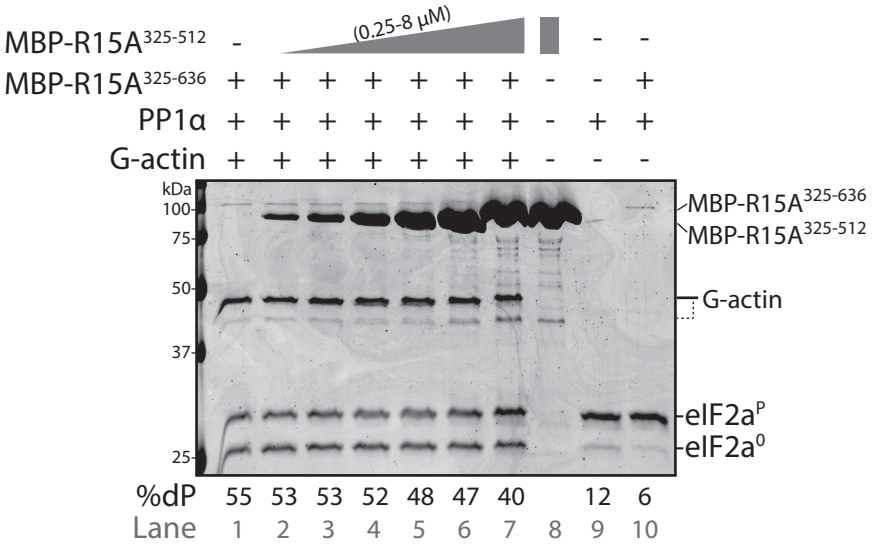
MBP-R15A325-512
(0.25-8 μM)
MBP-R15A325-636
PP1α
G-actin
kDa
100
75
50
37
25
MBP-R15A325-636
MBP-R15A325-512
G-actin
eIF2aP
eIF2a0
%dP 55 53 53 52 48 47 40 12 6
Lane 1 2 3 4 5 6 7 8 9 10

Figure 5

a

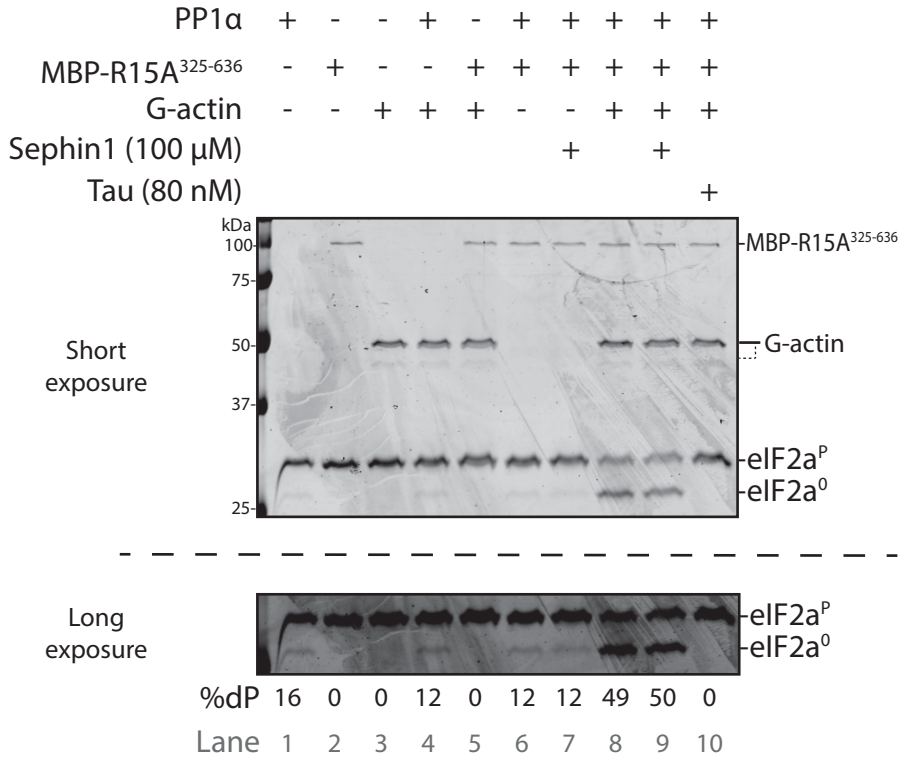
PP1α + - - + - + + + + +
MBP-R15A325-636 - + - - + + + + + +
G-actin - - + + + - - + + +
Sephin1 (100 μM) + +
Tau (80 nM) +
kDa
100
75
50
37
25
MBP-R15A325-636
G-actin
eIF2aP
eIF2a0
Short exposure
Long exposure
%dP 16 0 0 12 0 12 12 49 50 0
Lane 1 2 3 4 5 6 7 8 9 10

b

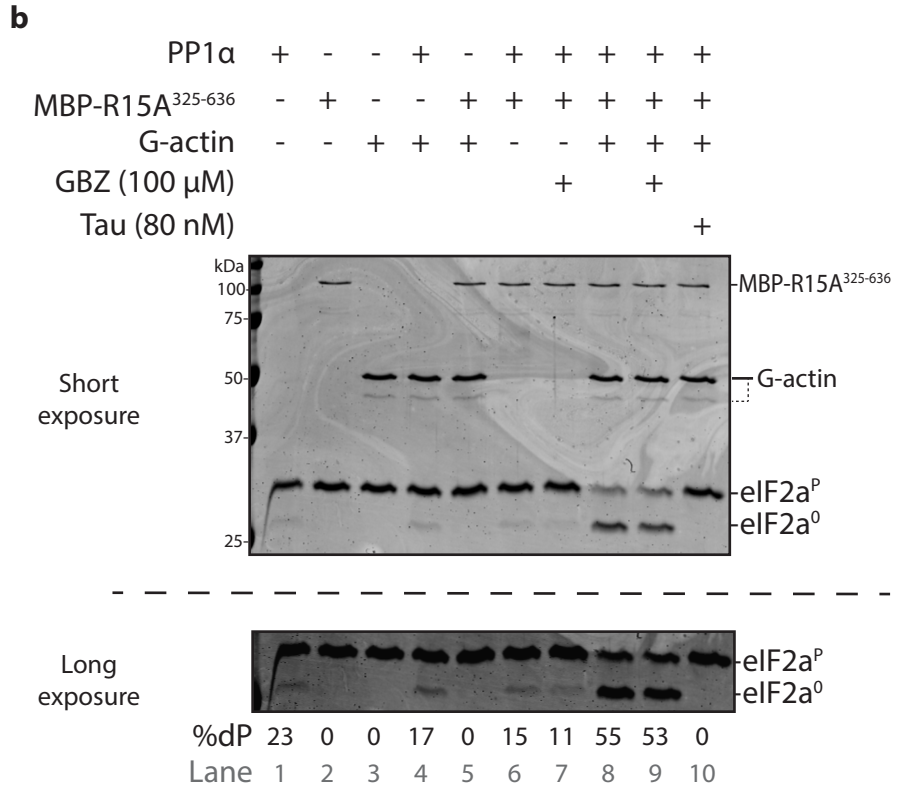
PP1α + - - + - + + + + +
MBP-R15A325-636 - + - - + + + + + +
G-actin - - + + + - - + + +
GBZ (100 μM) + +
Tau (80 nM) +
kDa
100
75
50
37
25
MBP-R15A325-636
G-actin
eIF2aP
eIF2a0
Short exposure
Long exposure
%dP 23 0 0 17 0 15 11 55 53 0
Lane 1 2 3 4 5 6 7 8 9 10

Supplementary Figure 1

a

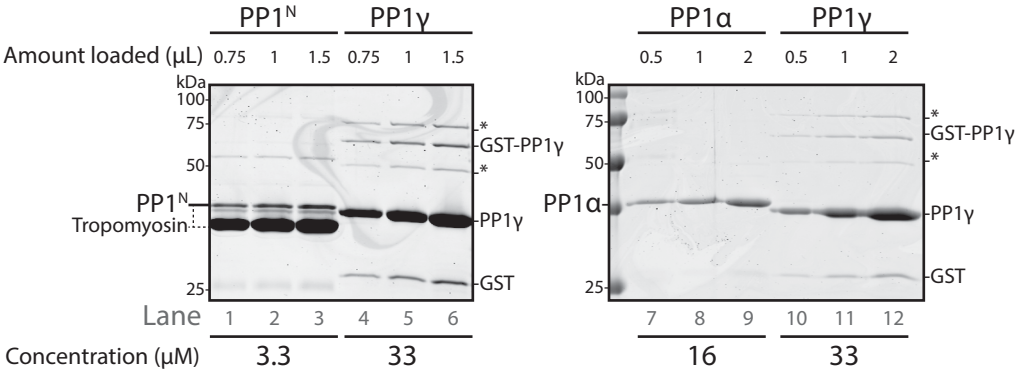

b

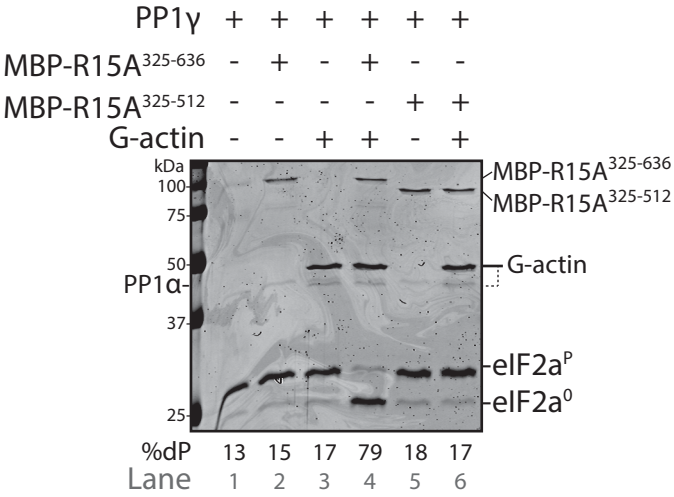

Supplementary Figure 2

a

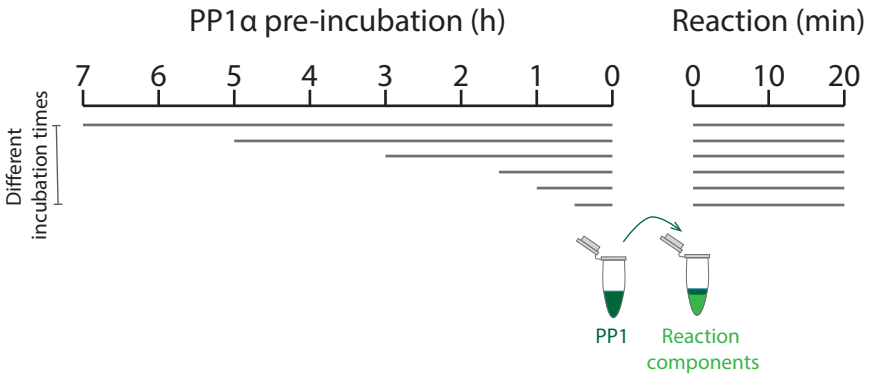

b

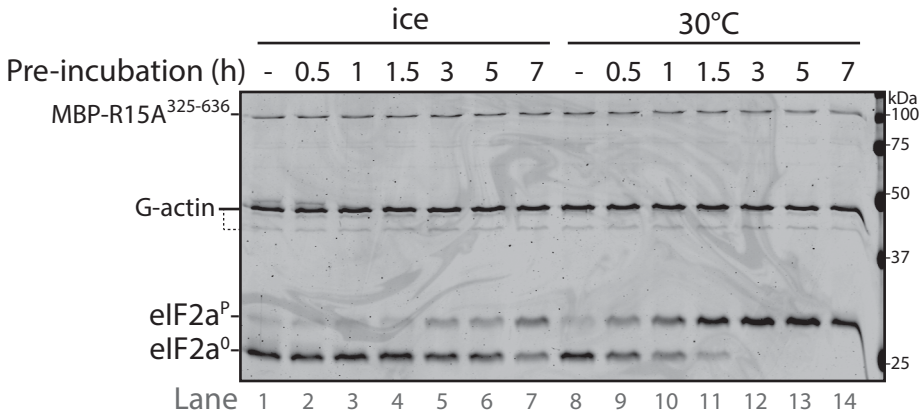

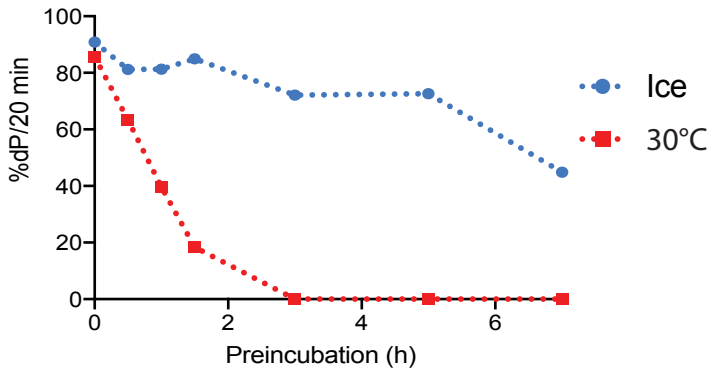

c

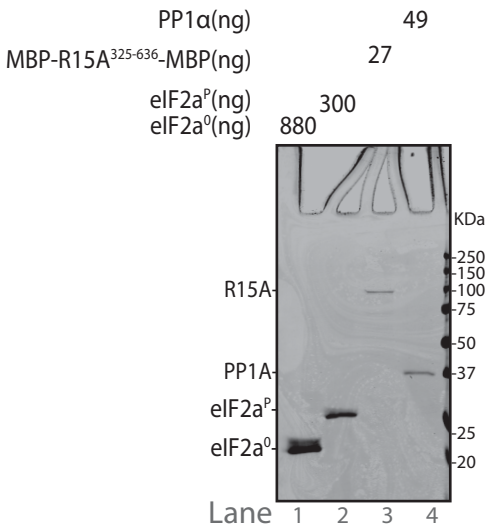

Supplementary Table 1 **Plasmids used in this study**

Lab number	Lab name	Description	Abbreviation	Reference
UK105	eIF2a-NM_pET30a	His6-tagged mouse eIF2a 1-185 pET-30a(+)"	eIF2a	PMID 15341733
UK168	PerkKD-pGEX4T-1	Bacterial expression plasmid for mouse PERK kinase domain	PERK	PMID 9930704
UK622	PGV_PP1G_1-323_V1	Bacterial expression plasmid for full-length PP1 phosphatase catalytic domain	PP1G	PMID 25774600
UK1920	huPPP1R15A_533_624_malE_pGEX_TEV_AviTag (MP1)	Bacterial expression plasmid for N-tern AviTagged human GADD34 533-624	R15A533-624-MBP	PMID: 28447936
UK1921	huPPP1R15A_325_636_malE_pGEX_TEV_AviTag (MP4	Bacterial expression plasmid for N-tern AviTagged human GADD34 325-624	R15A325-636-MBP	PMID: 28447936
UK2260	MBP_huPPP1R15A_325-636_H6_pMAL-c5X-His	Bacterial expression plasmid for MBP_R15A(325-636)-H6	MBP-R15A325-636	PMID: 28759048
UK2261	MBP_huPPP1R15A_325-512_H6_pMAL-c5X-His	Bacterial expression plasmid for MBP_R15A(325-512)-H6 (N-term)	MBP-R15A325-512	PMID: 28759048
UK2264	PP1A_7-330_RP1B (MPC)	Bacterial expression plasmid for H6-TEV-rabbit PP1A 7-330 Peti lab (Addgene Plasmid# 26566)	PP1a	PMID: 18992256

Supplementary Table 2

Figures		Repeats
1	a	4
	b	3
2	a	3
	b	3
	c	3
3	a	2
	b	2
4	a	n/a
	b	3
	c	2
5	a	3
	b	2
s1	a	1
	b	1
s2	a	n/a
	b	1
	c	2